Optimizing a Dynamical Decoupling Protocol for Nitrogen-Vacancy Center Ensembles

Supplemental Material

Coherence Curves

Full experimental coherence curves for the CPMG, XY8 and concatenated XY8 sequences at various numbers of pulses (8,72,584,4680 - according to the different concatenation levels) are shown in Fig. S1. The results for the KDD XY8 sequence, which was performed using different numbers of pulses (40,600,1000) are shown in Fig. S2. In all graphs, the vertical axis represents the contrast of the measurement, i.e. the contrast between the $m_s = 0$ and $m_s = 1$ states after final $\frac{\pi}{2}$ rotation of the spin state (see measurement description below). Each point represents an experiment with a fixed evolution time between the pulses. The measurement process is as follows:

1. Initialize the system at $m_s = 0$ using a ~ 50 μs 532−nm laser pulse and measure the reference fluorescence level N_{0i} during a ~ 2 μs window (in the $m_s = 0$ state).

2. Apply a $(\frac{\pi}{2}_x)$ $[(\frac{\pi}{2}_y)]$-pulse to rotate the spin state to the y $[x]$ axis. The rotation is performed on the Bloch-sphere, using IQ modulation of the MW signal.

3. Apply the DD pulse sequence.

4. Project the NV spin coherence into the $m_s = 0$ state: apply a final $(\frac{\pi}{2}_x)$ $[(\frac{\pi}{2}_y)]$-pulse to rotate the spin back to the lower part of the z axis and measure the fluorescence rate N_{0f} during a ~ 2 μs window at the beginning of a $\sim 50 - \mu s$ laser pulse.

5. Calculate the normalized fluorescence $n_0 = \frac{N_{0f}}{N_{0i}}$.

6. Repeat steps (1)-(5) 1000 times. The averaged result represents one measurement point in the coherence curve with a constant free evolution time between the pulses.

7. Repeat steps (1)-(6), only with the final NV spin coherence projected into the $m_s = 1$ state: the final $(\frac{\pi}{2})$-pulse is applied with an additional phase of 180^o to rotate the spin toward the lower part of the z axis. Calculate the normalized fluorescence $n_1 = \frac{N_{1f}}{N_{1i}}$. This additional step provides a complementary measurement to step 4, which allows for precise normalization of the data and common-mode rejection of noise.

8. Calculate the contrast between the n_0 and n_1 measurements: $C = \frac{n_0 - n_1}{n_0 + n_1}$. We refer to C as the absolute contrast of the measurement.

9. Change the free evolution time τ and repeat steps (1)-(8) to obtain 40 different measurement points along the coherence curve: 20 points are spread equally from the time $t = 0$ to the the longest desired experiment time $t = T$, and 20 additional points are taken at times shorter than the previous first point to improve the estimation for the initial contrast at short times. The free evolution time τ is swept in a random order (not just from the lowest to the highest) to avoid time-dependent systematic errors.

10. Repeat steps (1)-(9) 20 times to improve the signal to noise ratio for each measurement point and to avoid time-dependent systematic errors. The total time of a full DD experiment is $\sim 4 \times 10^5 \times T$, where T is longest time of a single sequence in the resulting coherence curve (e.g., for a sequence with 584 pulses, 35 $ms \times 4 \times 10^5 \sim 4$ hours).

Each data set is fitted to a stretched exponential of the form $f(x) = Ae^{-(\frac{x}{T_2})^\beta}$, where A represents the initial absolute contrast at short times, T_2 is the extracted coherence time and β is the stretching factor of the exponential. Finally, the graphs were normalized to the initial absolute contrast of a Hahn-Echo experiment.

It is clearly seen from Fig. S1 and Fig. S2 that for a given number of pulses, CPMG provides the best coherence time and initial contrast along the x axis, but the CPMG contrast vanishes completely along the perpendicular axis. All other sequences perform similarly for initializing along S_x and S_y.

Before starting to work with and modify the XY8 sequence, we also examined the performance of other XY-based sequences, namely XY4 (Fig. S3) and XY16 (Fig. S4). In both sequences the initial contrast at short times drops faster than XY8 with the number of pulses. Generally, we would expect that a more symmetrized sequence will result in a better contrast (meaning that XY4 contrast $<$ XY8 contrast $<$ XY16 contrast). However, the contrast drop of XY16 is faster than XY8. We suspect that this is because the XY16 sequence introduces additional $-x$ and $-y$ pulses, which have additional pulse errors and are not necessarily perpendicular to the y and x axes respectively, as required in XY16.

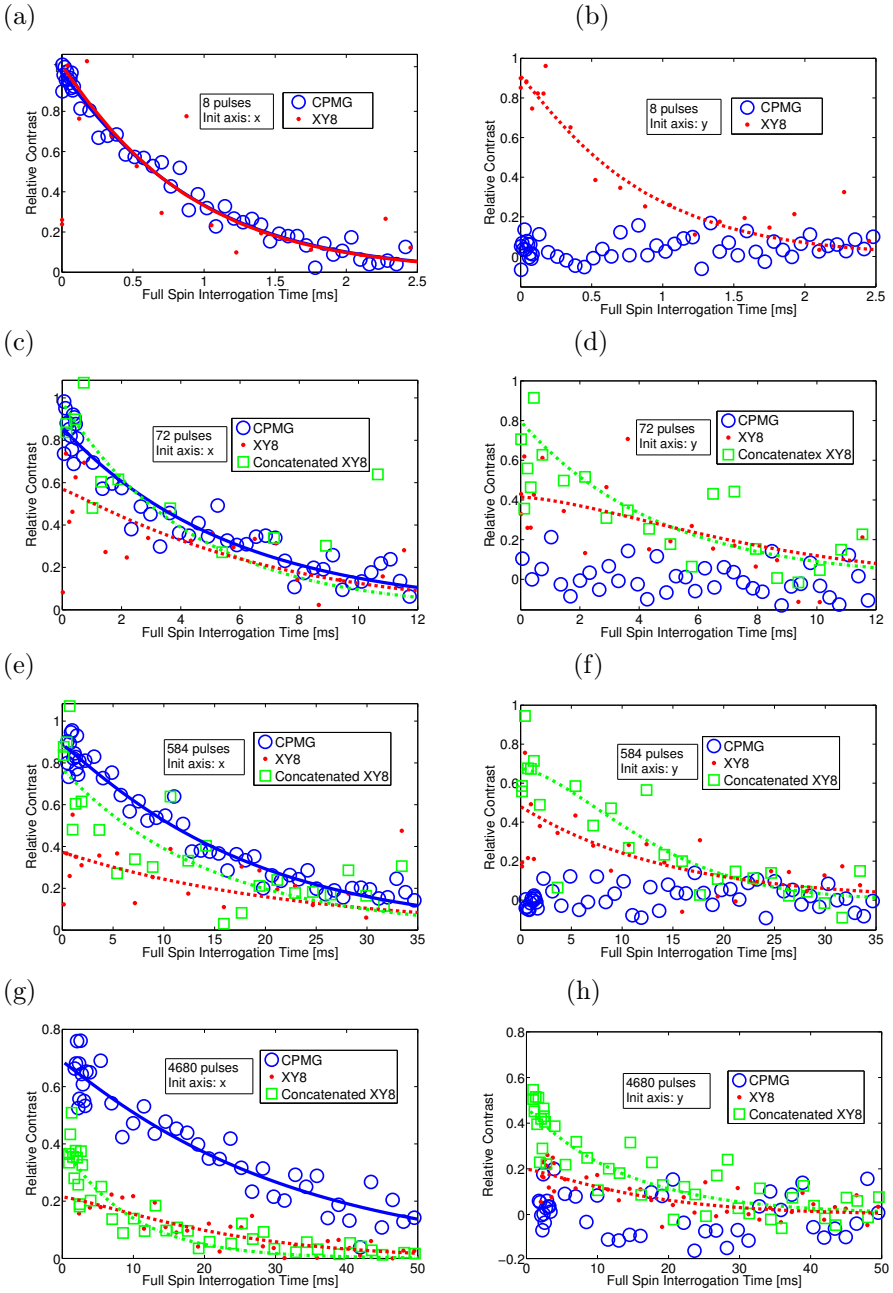

Figure S1: Full coherence curves for the CPMG (blue, solid lines), XY8 (red, dashed lines) and concatenated XY8 (green, dash-dotted lines) sequences. At 8 pulses, the concatenated sequence is identical to regular XY8 (this is level 0 of concatenation). (a) 8 pulses, initialized along the x axis (b) 8 pulses, initialized along the y axis (c) 72 pulses, initialized along the x axis (d) 72 pulses, initialized along the y axis (e) 584 pulses, initialized along the x axis (f) 584 pulses, initialized along the y axis (g) 4680 pulses, initialized along the x axis (h) 4680 pulses, initialized along the y axis .

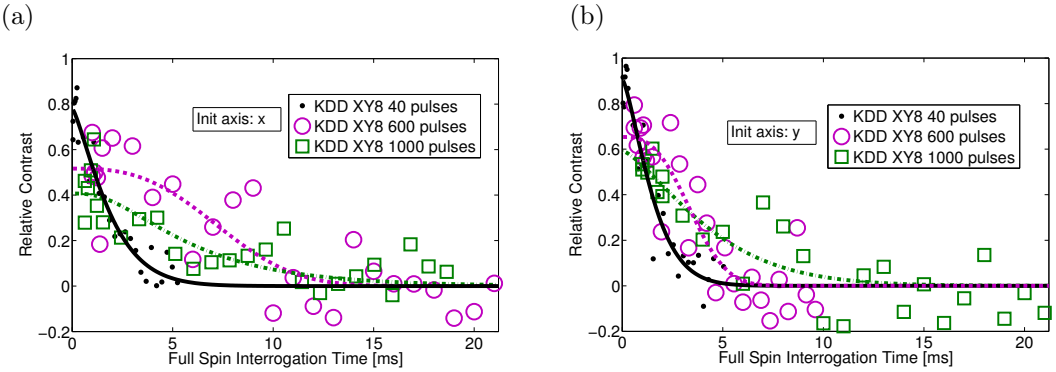

Figure S2: Full coherence curves for the KDD XY8 sequence, at 40 (black, solid lines), 600 (purple, dashed lines) and 1000 (green, dash-dotted lines) pulses. (a) initialization along the x axis (b) initialization along the y axis.

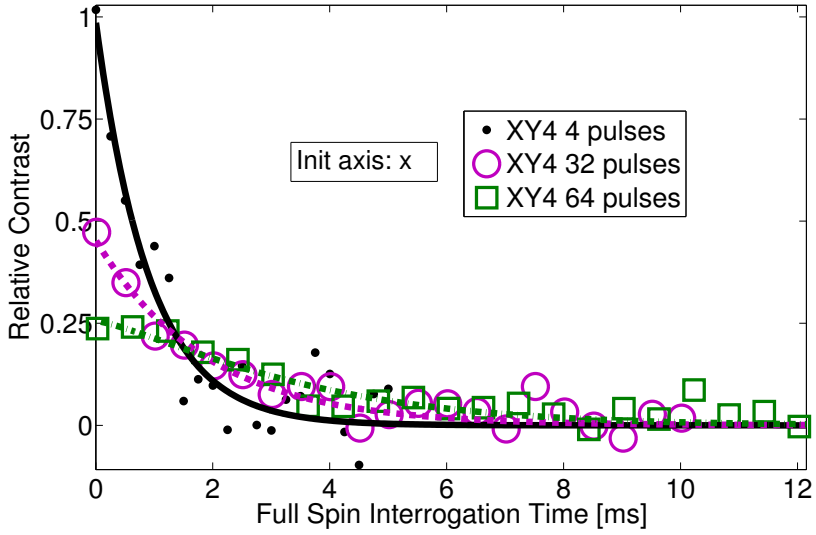

Figure S3: Full coherence curves along the x axis for the XY4 sequence, at 4 (black, solid lines), 32 (purple, dashed lines) and 64 (green, dash-dotted lines) pulses.

Initial Contrast Simulation

Let us now explain the simulations in Fig. 3(a) in the main text. One of the errors that result in the contrast drop is caused by the hyperfine structure [Fig. 1(c) in the main text]. This hyperfine structure results from interactions with ^{14}N nuclear spins and also contains artifacts arising from strain inhomogeneities. We work with a MW driving frequency of 3.2078 GHz, which corresponds to the main dip in the hyperfine structure. The hyperfine structure suggests two

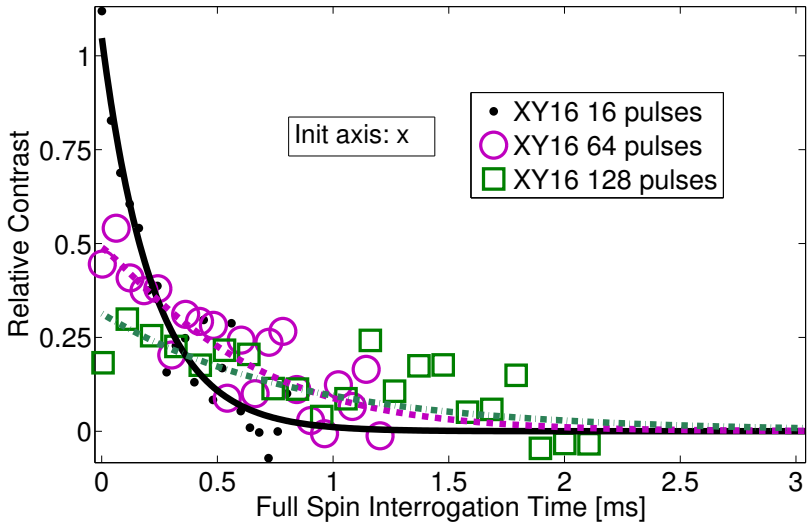

Figure S4: Full coherence curves along the x axis for the XY16 sequence, at 16 (black, solid lines), 64 (purple, dashed lines) and 128 (green, dash-dotted lines) pulses.

additional frequencies that are detuned from this frequency by $\delta \sim 2.2$ and $\delta \sim 4.4$ MHz. We estimate the populations of the detuned spins from the hyperfine structure [Fig. 1(c)]: 70% with no detuning, 20% with $\delta = 2.2$ MHz and 10% with $\delta = 4.4$ MHz. We therefore model the detuning in the hyperfine structure by a distribution consisting of three Gaussians, which are centered around the detuning frequencies, having a standard deviation of ~ 0.5 MHz and proper weights as descrived above. For each NV center in each realization, we generate a detuning value from this distribution and take it into account in the contrast simulation (by plugging it into Eq. 2 of the main text) as the n_z error. We then ensemble-average over 10^4 NV centers with randomly chosen detunings, to obtain the simulation results at Fig. 3(a). Having a measured Rabi frequency of ~ 14 MHz, the simulation produces similar results as if the detuning was chosen randomly from an effective Gaussian distribution around 0 with a standard deviation of $n_z = \frac{0.7\times 0+0.2\times 2.2+0.1\times 4.4}{14} \sim 0.06$.

The rotation axis also deviates from the desired one due to phase errors. The measured phase accuracy of the signal generator used in the experiment (SRS SG384) at a frequency of ~ 3 GHz is $\sim 3°$, and the minimal phase difference between adjacent pulses (in KDD) is not longer than 60°, causing a possible rotation axis error of $n_{xy\perp} = \frac{3}{60} \sim 0.05$. This error is taken into account as a possible rotation axis error around the $x - y$ plane, e.g. if a pulse is applied along the x axis, it may have a rotation element of ~ 0.05 around the y axis. In such a case, the rotation axis used in the contrast simulation

(Eq. 1 in the main text, which is later plugged into Eq. 2) is therefore $\hat{n} = n_z\hat{z} + n_{xy\perp}\hat{y} + \sqrt{1 - n_{xy\perp}^2 - n_z^2}\,\hat{x}$. Furthermore, such phase errors are more significant in the KDD sequence (phase difference between adjacent pulses is sometimes 60°) than in the other sequences (phase difference between adjacent pulses is not smaller than 90°), and thus may have a non-negligible effect on the ability to increase the coherence time [see the underperformance of the KDD sequencse in Fig. 3 (b) of the main text]. The analysis of these effects requires simulating the full behavior of the coherence curve, which is beyond the scope of this work, and will be discussed in a future theoretical work.

Another effect that reduces the contrast is temporal deviations from perfect (π)-pulses, represented by an error in the roataion angle. The timing resolution of the TTL pulse generator (PulseBlasterESR-PRO-500) is 2 ns. The measured (π)-pulse duration is 36 ns, thus the angle error can be $\frac{2}{36} \sim 0.055$. The rotation angle is also affected by the inhomogeneity of the MW and static magnetic field over the measurement volume. The intensity of the MW field is proportional to $\frac{1}{r}$, where r is the distance to the symmetry axis of the MW wire. Since the closest distance from the measurement volume to this axis is 93.5 μm and the farthest distance is 96.5 μm, this inhomogeneity is about 2%. Combining this effect with the TTL timing resolution results in a total angle error of $\epsilon = \sqrt{0.055^2 + 0.02^2} \sim 0.06$. The inhomogeneity of the static field, placed in a distance in the order of centimeters from the measurment light spot is negligible.

We use Eq. (2) of the main text to simulate the contrast in the theoretical limit of $T \to 0$. In this regime, the evolution time τ is also short, there is no decoherence, hence the free evolution operators between pulses are unity, and the initial contrast is just a multiplication of rotation operators of the form $U_{\hat{k}i}$. In the simulation, we assume that different NVs in the ensemble feel different pulse and detuning errors. For each NV center, we generate random axis and angle errors from Gaussian distributions with standard deviations of $n_z = 0.06$, $n_{xy\perp} = 0.05$ and $\epsilon = 0.06$ respectively, and calculate the contrast according to Eq. (2). We average out the results of 10^4 NV centers to obtain the simulation at Fig. 3(a) of the main text.

Despite providing a qualitative agreement, the simulations do not predict the experimental outcome [Fig. 3(b)] quantitatively. We suspect that the interplay between pulse errors and additional effects of decoherence and inhomogeneous broadening, which were not taken into account in the simulations, may have an additional effect on the contrast drop. This will be the main topic of a future study.

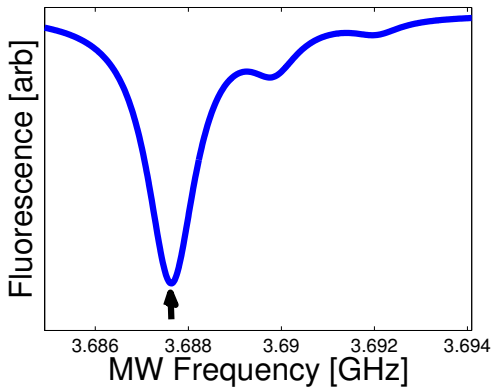

Figure S5: Optically detected magnetic resonance measurement of $|0\rangle \leftrightarrow |+1\rangle$ transition in an NV ensemble, with better alignment of a static ~ 300 G magnetic field, creating higher polarization of the ^{14}N nuclear spins into the $|-1\rangle$ spin state.

Measurements at different conditions

In order to verify the validity of our results, we repeated the experiment (the CPMG, XY8 and concatenated XY8 sequences) at slightly different conditions: the light spot was focused on a different region of the diamond sample, the obtained Rabi frequency was ~ 10 MHz and the alignment of the static magnetic field was improved to achieve higher polarization of the ^{14}N nuclear spins into the $|-1\rangle$ spin state (as seen in Fig. S5), reducing the effects of detuning. The results for the coherence time and relative contrast with the number of pulses are summarized in Fig. S6. For all the sequences, the relative contrast levels [Fig. S6 (a)] are slightly higher than in the previous data set [Fig. 3 (b)], probably due to the higher polarization level of the nuclear spins, but the coherence times [Fig. S6 (b)] are slightly lower, probably due to higher N concentration at the measurement volume.

Contrast measurements as a function of (π)-pulse duration (axis error)

We performed measurements of the XY8 contrast at short times with varying numbers of pulses at both experimental conditions. We reduced the intensity of the MW field, resulting in longer (π)-pulse durations. For each intensity, we performed Rabi spectroscopy to determine the correct duration of (π)-pulses, later to be used in the contrast measurements. Longer (π)-pulses, resulting from weaker MW fields, represent higher axis errors. We measured the XY8 contrast at the various intensities, to experimentally determine the dependence of the contrast on the (π)-pulse duration.

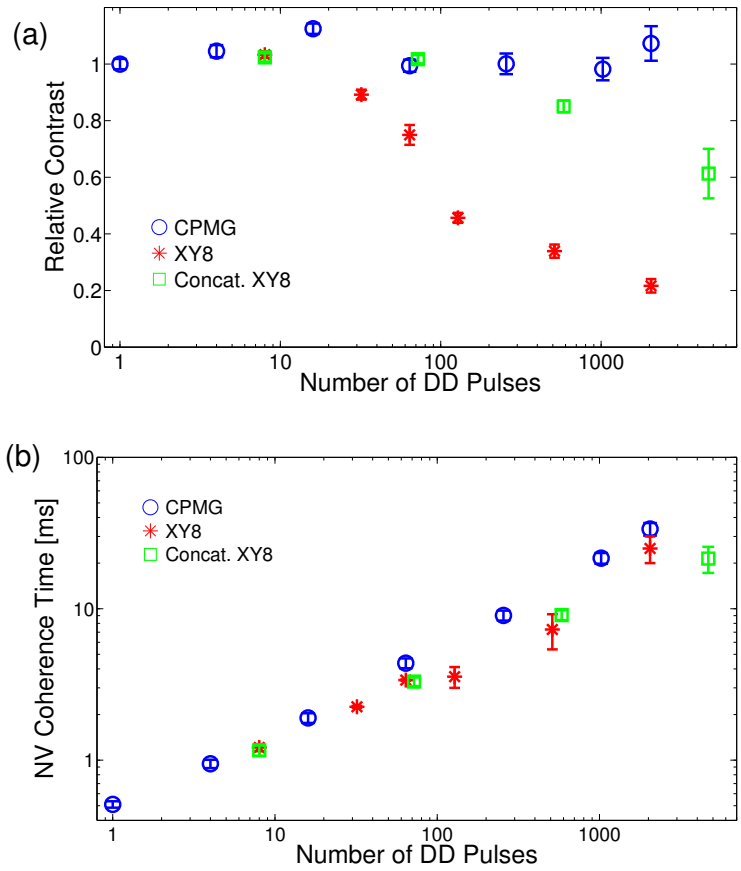

Figure S6: (a) Relative contrast in the decoherence-free limit ($\tau \ll \frac{T_2}{n}$) of DD protocols as a function of number of pulses for the second data set. (b) The coherence time of DD sequences as a function of the number of pulses for the second data set.

The results are summarized in Fig. S7. It is clear that for the first data set, the contrast decreases significantly with the (π)-pulse duration, while for the second data set, the contrast does not change with the (π)-pulse duration, due to the better nuclear polarization, meaning that the axis error for the latter case is much lower. However, even for the latter case, the contrast drops with the number of pulses in a way that our simulations do not explain, demonstrating the importance of theoretically analyzing the interplay between pulse errors and decoherence effects, which will be done in a future work.

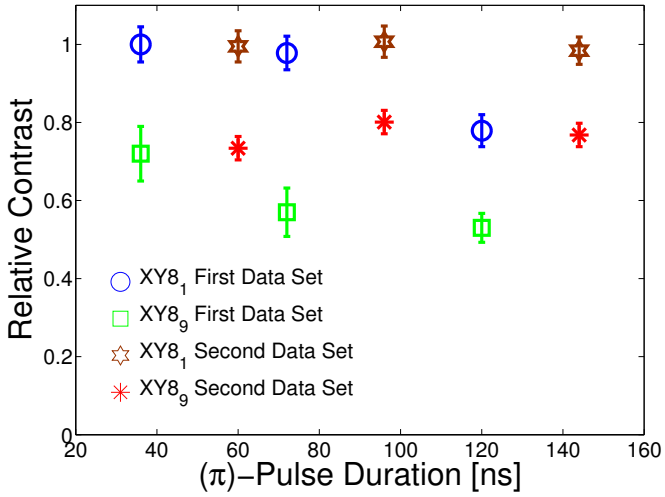

Figure S7: Relative contrast in the decoherence-free limit ($\tau \ll \frac{T_2}{n}$) as a function of (π)-pulse duration for two experimental configurations: the first one with the hyperfine structure shown in Fig. 1(c) of the main text, the second one with the hyperfine structure shown in Fig. S5. The results are shown for $XY8_1$ (8 pulses) and $XY8_9$ (72 pulses).

Contrast measurements as a function of timing deviation (angle error)

We investigated the dependence of the XY8 contrast at short times on the temporal errors. By performing Rabi spectroscopy, we determined the correct duration of (π)-pulses. Then, we applied the XY8 sequence with varying number of pulses, whose durations were intentionally shifted from the correct (π)-pulse durations, effectively creating larger angle errors. We measured the contrast at short times for different inaccurate MW pulse durations. The results (Fig. S8) demonstrate that as the number of pulses increases, it is much more critical to maintain accurate (π)-pulses. However, even at low numbers of pulses where a good temporal resolution is not necessary, the contrast still decreases with the number of pulses, which requires further theoretical understanding of decoherence at short times.

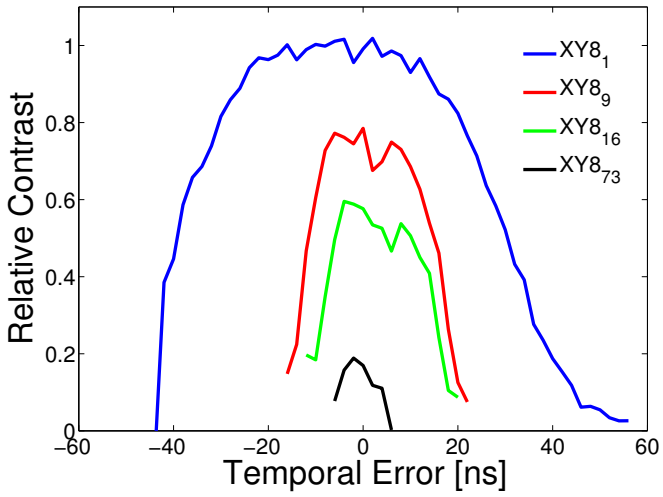

Figure S8: Relative contrast in the decoherence-free limit ($\tau \ll \frac{T_2}{n}$) as a function of temporal deviation from a correct (π)-pulse. The results are shown for $XY8_1$ (8 pulses), $XY8_9$ (72 pulses), $XY8_{16}$ (128 pulses) and $XY8_{73}$ (584 pulses).